Submitted

The impact trajectory of asteroid 2008 TC_3

Davide Farnocchia*[a], Peter Jenniskens[b], Darrel K. Robertson[c], Steven R. Chesley[a], Linda Dimare[d], Paul W. Chodas[a]

ABSTRACT

Asteroid 2008 TC_3 was the first asteroid ever discovered before reaching Earth. By using the almost 900 astrometric observations acquired prior to impact we estimate the trajectory of 2008 TC3 and the ground-track of the impact location as a function of altitude. For a reference altitude of 100 km the impact location 3-σ formal uncertainty is a 1.4 km $\times$ 0.15 km ellipse with a semimajor axis azimuth of 105°. We analyze the contribution of modeling errors and find that the second-order zonal harmonics of the Earth gravity field moves the ground-track by more than 1 km and the location along the ground-track by more than 2 km. Non-zonal and higher order harmonics only change the impact prediction by less than 20 m. The contribution of the atmospheric drag to the trajectory of 2008 TC_3 is at the numerical integration error level, a few meters, down to an altitude of 50 km. Integrating forward to lower altitudes and ignoring the break-up of 2008 TC_3, the atmospheric drag causes an along-track error that can be as large as a few kilometers at sea level. The locations of the recovered meteorites is consistent with the computed ground-track.

Subject headings: astrometry; celestial mechanics; minor planets, asteroids: individual (2008 TC_3)

1. Introduction

Asteroid 2008 TC_3 was discovered by R. Kowalski (MPEC 2008-T50)[1] at the Mt. Lemmon station of the Catalina sky survey (Larson et al. 1998) on 2008-Oct-06 at 06:40 UTC. The plane-of-sky rate of motion $> 6''$/min immediately suggested that the object was likely a near-Earth asteroid

*Davide.Farnocchia@jpl.nasa.gov

[a]Jet Propulsion Laboratory, California Institute of Technology, Pasadena, CA 91109, USA

[b]SETI Institute, Mountain View, CA 94043, USA

[c]NASA Ames Research Center, Moffett Field, CA 94035, USA

[d]SpaceDyS s.r.l., 56023 Cascina, PI, Italy

[1]http://www.minorplanetcenter.net/iau/mpec/K08/K08T50.html

and so Kowalski rapidly obtained follow-up observations. After receiving additional observations from the Sabino Canyon Observatory, the RAS Observatory in Moorook, and the Siding Spring Survey, the Minor Planet Center announced the discovery of 2008 TC_3 and reported that the nominal trajectory corresponded to an Earth impact on 2008 Oct 7, only 20 hours after discovery (MPEC 2008-T50). The absolute magnitude $H = 30.4$ of the asteroid suggested a size of a few meters. NASA's Jet Propulsion Laboratory confirmed the impact prediction and indicated the Nubian Desert in North Sudan as the impact location.[2]

As 2008 TC_3 was recognized as an impactor and thanks to the favorable observing geometry, astronomers all over the world started tracking the object and managed to obtain almost 900 observations up to an hour before impact,[3] which helped refine the impact location and time estimates. Jenniskens et al. (2009) successfully conducted a campaign to search for the 2008 TC_3 meteorites and managed to recover 600 meteorites with a total mass of 10.7 kg (Shaddad et al. 2010), which landed on the ground after the asteroid exploded at an altitude of 37 km. The subsequent analysis of the meteorites indicated that the asteroid was an achondrite belonging to the spectral class F (Tholen 1989) and that its diameter was about 4 m, if a low albedo object (Jenniskens et al. 2009; Kozubal et al. 2011; Kohout et al. 2011).

The available astrometric dataset and the known location of the meteorites provide strong and essentially unique observational constraints to test the accuracy of the models used for orbit determination and impact location and time estimation. To date only a second asteroid has been discovered before impact, 2014 AA (MPEC 2014-A02).[4] However, the available observational information for 2014 AA is limited to seven astrometric positions and an infrasound detection of its atmospheric entry. Therefore, the impact footprint has a larger uncertainty of 141 km × 10 km (1-σ, Farnocchia et al. 2016) than that of 2008 TC_3.

2. Orbit determination

The 883 astrometric observations available for 2008 TC_3 provide very significant constraints on the orbit despite an observed arc of only 19 h. The least-squares solution (JPL solution 18) is shown in Table 1 along with the formal 1-σ uncertainties in the orbital elements.

[Table 1 about here.]

Figure 1 shows the astrometric Right Ascension and Declination residuals against solution 18. It is clear how the astrometric quality degrades as we get closer to the impact. Part of the problem

[2] http://neo.jpl.nasa.gov/news/news159.html

[3] http://www.minorplanetcenter.net/tmp/2008_TC3.txt

[4] http://www.minorplanetcenter.net/mpec/K14/K14A02.html

is due to the plane-of-sky velocity of 2008 TC_3, which becomes as large as $12''$/s an hour before impact. Therefore, small timing errors can result in significant astrometric position errors in the along-track direction, i.e., the direction corresponding to the plane-of-sky motion. As shown in the top panel of Fig. 2, along-track residuals become of the order of $10''$ at the end of the observed arc. Though they are smaller than the along-track errors, large residuals of the order of $3''$ also occur in the cross-track direction, see bottom panel of Fig. 2. The increase of the cross-track errors is likely due to the increasing brightness of 2008 TC_3, which reaches a V-band magnitude of 13 at the end of the arc, thus making it difficult to accurately measure its astrometric position.

[Figure 1 about here.]

[Figure 2 about here.]

To mitigate the effect of star catalog systematic errors, we applied the Farnocchia et al. (2015a) debiasing scheme. Corrections were as large as $0.5''$, in particular for astrometric positions reduced against the USNO-A2.0 catalog (Monet 1998). To assign the data weights we accounted for both the expected quality for given observers (e.g., $0.5''$ for Kowalski's observations) as well as the internal consistency of batches of observations coming from the same observatory. In particular, observations toward the end of the arc were deweighted to account for the degrading quality shown in Fig. 1 and Fig. 2. Finally, we removed from the fit batches of observation from the same station that appeared to be consistently biased for a total of 308 rejections. The resulting reduced χ^2 of the least-squares fit (e.g., Taylor 1997) is 0.39.

The force model we used includes the Newtonian gravitational attraction of the Sun, eight planets, Pluto, and the Moon based on JPL's Planetary and Lunar Ephemerides DE431 (Folkner et al. 2014). Moreover, we added the contribution of the 16 most massive main-belt bodies (e.g., Farnocchia et al. 2015b). For relativity, we used the Einstein-Infeld-Hoffmann formulation, which also accounts for the relativistic terms of the planets (Moyer 2003, Sec. 4). Finally, to account for the effect of the Earth oblateness, we added the quadrupole term of the geopotential (Kaula 1966) with $J_2 = 0.00108263$ (Folkner et al. 2014).

3. Impact and drag-free ground-track

Table 2 shows the impact parameters at a reference altitude $h = 100$ km along with the corresponding uncertainties for the orbit presented in Sec. 2. All the reported quantities in Table 2 and throughout the paper are referred to the World Geodetic Reference 1984 ellipsoid[5] and an Earth rotation model based on JPL's Earth Orientation Parameters (EOP, Chin et al. 2009),[6]

[5] http://earth-info.nga.mil/GandG/publications/tr8350.2/wgs84fin.pdf

[6] http://keof.jpl.nasa.gov/

which model irregularities in the Earth rotation and provide corrections with respect to the 1980 IAU Theory of Nutation (Seidelmann 1982). The impact is above the Nubian Desert in North Sudan and velocity relative to the observer at the impact location has a magnitude of 12 km/s with an entry angle (Elevation) of 21°. From the impact location, 2008 TC_3 is seen arriving from an azimuth of 281°, i.e., from the west direction with an 11° angle with respect to the local parallel.

[Table 2 about here.]

2008 TC_3 exploded at an altitude of about 37 km and meteorites reached the ground (Jenniskens et al. 2009). Table 3 and Fig. 3 give the 2008 TC_3 ground-track, i.e., the projection on the ground of longitude and latitude as function of the altitude as the trajectory reaches the ground.

[Table 3 about here.]

[Figure 3 about here.]

As the impact altitude decreases, the impact location uncertainty ellipse remains close to that corresponding to $h = 100$ km: the ellipse semiminor axis remains constant, the semimajor axis and the major axis azimuth change a rate of about +0.5 m and +0.007° per 1 km of altitude, respectively, thus becoming 0.514 km and 105.2° at sea level.

As shown by Figure 4, the ground-track and the meteorite locations are consistent. The larger meteorites nicely scatter around the ground-track while the smaller ones show a south offset with respect to the ground-track, which is likely caused by winds at the time of the atmospheric entry of 2008 TC_3 (see Sec. 4.3).

[Figure 4 about here.]

4. Sensitivity analysis

To test the robustness of the orbit solution and impact prediction presented in Sec. 2 and Sec. 3 we performed a sensitivity analysis to assess possible inaccuracies due to the adopted modeling setup.

4.1. Statistical treatment of the astrometry

We considered each of the following data treatment variations with respect to the nominal one discussed in Sec. 2:

- To test the effect of the Farnocchia et al. (2015a) star catalog debiasing we computed a solution with no debiasing;
- To test the sensitivity to the manually chosen outliers we computed a solution where the outliers were automatically selected by using the Carpino et al. (2003) algorithm with a rejection threshold $\chi_{rej} = 3$;
- To test the sensitivity to the adopted data weights we computed a solution with uniform weighting at $1''$;
- To test the sensitivity to the data arc we computed a solution with data cutoff on 2008 Oct 07.0 UTC.

For the baseline solution of Sec. 2 as well as these alternate orbital solutions, Fig. 5 and Fig. 6 show the predictions for impact location and time along with their 3-σ uncertainties for an altitude of 100 km. All the solutions give statistically consistent predictions, e.g., the short-arc 3-σ uncertainty contains that of the long-arc solutions. This overall consistency gives us confidence that the orbital solution is not significantly altered by the adopted statistical treatment of the astrometry.

The effect of debiasing is quite small, 38 m, which can be expected. First, star catalog systematic errors get randomized by the different catalogs used to reduce the astrometry and the rapidly changing plane-of-sky location of 2008 TC_3. Moreover, orbital dynamics and the extent of the observed arc eventually control the trajectory rather than observational biases. It is interesting to note how using the Farnocchia et al. (2015a) debiasing scheme produces a better fit to the astrometric observations, i.e., the least-squares fit has a $\chi^2 = 71.1$, while without debiasing we obtain $\chi^2 = 74.4$. Since the trajectories do not differ significantly, this lower χ^2 is a further confirmation that the debiasing scheme gives more accurate astrometric positions.

The solution with manual rejection of outliers differs from that with automatic rejection of outliers by less than 1σ. The only significant discrepancy, about 3σ, is that between JPL solution 18 and the solution computed with uniform weights at $1''$. However, Fig. 1 shows that $1''$ is not a realistic assumption for the astrometric errors, which could cause this latter solution to deviate from the others.

[Figure 5 about here.]

[Figure 6 about here.]

4.2. Atmospheric drag

For lower altitudes, the main source of uncertainty in the impact location estimate comes from atmospheric drag, which slows and displaces 2008 TC_3 as it enters the Earth atmosphere. Modeling

of the drag accelerations is possible because there is knowledge of the 2008 TC_3 shape, rotation state, orientation during impact, composition as well as the atmospheric winds and atmospheric profile at the time of the atmospheric entry.

The shape and rotation of 2008 TC_3 were derived from oscillations of the observed brightness and there are two near-mirror solutions (Scheirich et al. 2010). For this simulation we only used the first solution. The shape of 2008 TC_3 was extracted from the Database of Asteroid Models from Inversion Techniques (DAMIT, Ďurech et al. 2010). The values for inertia and angular momentum in the DAMIT database did not agree with those published in Scheirich et al. (2010). Upon request, Ďurech was able to provide the correct inertia values, $(I_{xx}/I_{zz}, I_{yy}/I_{zz}) = (2.79, 3.2)$, and angular momentum, $L/I_{zz} = 693.202593$ Hz. The orientation was re-derived by calculating the reflected light observed at Earth from the shape model using the method of Kaasalainen and Torppa (2001) and comparing to the lightcurve given in the DAMIT. Integration of the rotational state using a 4th order or higher Runge-Kutta scheme then provided excellent agreement with the observed lightcurve (Fig. 7).

[Figure 7 about here.]

The integration was then continued from the time when 2008 TC_3 entered Earth's shadow and observations ceased until it entered Earth's atmosphere at an altitude of 100 km on 2010 Oct 07 at 02:45:30 UTC. The rotational and precession period are both about 100 s so the rotation speed was ignored for the few seconds of entry when atmospheric pressure quickly takes over. Table 4 gives the corresponding orientation of 2008 TC_3 at entry. For entry over 100 km altitude at longitude 30.5380°, latitude 21.0871° with trajectory from a direction azimuth 101.0968° and elevation 20.8332° (Table 2), the orientation of the body axis in terms of the Direction Cosine Matrix can be rotated into the Ground Range Frame, defined by directions Uprange, Crossrange, and Zenith (Table 4).

[Table 4 about here.]

The highest uncertainty in the drag coefficient comes from the unknown albedo of 2008 TC_3. The absolute magnitude was $H = 30.86 \pm 0.01$ with slope parameter $G = 0.33 \pm 0.33$ (Kozubal et al. 2011). Other constraints on the kinetic energy and diameter of the asteroid suggest that 2008 TC_3 had a relatively low density of 1.8 g/cm^3 and albedo $p_V = 0.046 \pm 0.005$ (Kozubal et al. 2011; Kohout et al. 2011). However, the albedo of recovered meteorites were of order 0.088 ± 0.015 (Jenniskens et al. 2009). The longest axis of the asteroid scaled as $1.15\sqrt{p_V}$, with an axis ratio of $1 : 0.54 : 0.36$ (Kozubal et al. 2011; Scheirich et al. 2010).

We adopted the low albedo size of $5.4 \times 4.3 \times 3.4$ m. The drag coefficient for this model was obtained from a simulation of the entry using the ALE3D hydrocode from Lawrence Livermore

National Laboratory.[7] Combined with an entry angle of 20.833, we used the Ground Range Frame orientation as a starting point for a hydrocode simulation that followed the asteroid down through the atmosphere from an initial altitude of 70 km through breakup.

For the force calculation the body can be rotated into the Wind Frame (Drag, Side, Lift directions), as shown in Fig. 8. The cross-sectional areas in the wind frame are [10.5, 8.94, 17.5] m^2. Using these as the reference areas the drag, lift, and side-force coefficients were calculated during the first second of entry. Beyond 1 s, the shape begins to rotate and deform noticeably (see Fig. 9).

[Figure 8 about here.]

[Figure 9 about here.]

The coefficients are given by the force F divided by the dynamic pressure and the cross-sectional area A in each direction. The dynamic pressure comes from the density of the atmosphere at the altitude $\rho_{\rm atm}$ at each time, and the average net velocity $\mathbf{v}$ of the asteroid at that time (Roy 2005, Chap. 11):

$$C = \frac{F}{qA} \quad , \quad q = \frac{1}{2}\rho_{\rm atm}|\mathbf{v}|^2 \ .$$

The drag coefficients evolve as the asteroid penetrates the atmosphere from changes in orientation and shape (see Table 5). The drag coefficient stays about 1.9 prior to deformation, but the side force and lift both swap directions.

[Table 5 about here.]

The single-strength hydrodynamic model is not an accurate representation of the behavior of 2008 TC_3 in the atmosphere. In reality, the asteroid showed significant disruption at around 42, 37 and 33 km altitude. To model drag we used the drag equation (Roy 2005, Chap. 11):

$$\mathbf{a}_{\rm drag} = -\frac{1}{2}\rho_{\rm atm}|\mathbf{v}|C_D\frac{A}{M}\mathbf{v} \tag{1}$$

where $\rho_{\rm atm}$ is the atmospheric density, $\mathbf{v}$ is the velocity of 2008 TC_3 relative to the atmosphere, A and M are the cross-sectional area and mass of 2008 TC_3, respectively. From Jenniskens et al. (2009) we have $A = 13.2$ m^2 and $M = 83$ t. For simplicity, we set the drag coefficient C_D to a constant value 1.8. The atmospheric density as a function of the altitude is based on the COSPAR International Reference Atmosphere 2012.[8]

[7] https://wci.llnl.gov/simulation/computer-codes/ale3d

[8] http://spaceweather.usu.edu/files/uploads/PDF/COSPAR_INTERNATIONAL_REFERENCE_ATMOSPHERE-CHAPTER-1_3%28rev-01-11-08-2012%29.pdf

Figure 10 shows the along-track and cross-track differences between the drag-free solution and the one that includes drag. Figure 11 shows the differences in the velocity relative to the impact point. To quantify the effect of drag at lower altitudes we ignored the explosion and integrated through 0 km altitude. Down to about 50 km the differences are at the numerical noise level, then the velocity relative to the impact point decreases rapidly and so the trajectory perturbed by drag is trailing the drag-free trajectory with an along-track error that becomes as large a 3.7 km at sea level. The cross-track differences become visible at an altitude of about 10 km and become as large as 23 m at sea level.

[Figure 10 about here.]

[Figure 11 about here.]

4.3. Winds

The influence of winds is evaluated from the UK Meteorological Offce (UKMO) wind model (Swinbank and O'Neill 1994) over the fall area at that time (Shaddad et al. 2010, Fig. 4). The UKMO model showed that winds were relatively mild below 30 km altitude, less than 9 m/s, and were blowing predominantly to the North above 5 km altitude, but reversed direction to the South at lower elevations. As a result, meteorites tend to drift initially North of the trajectory, then reverse course and drift almost all the way back, independent of size. For a spherical meteorite, the typical displacement is 100-m North of the approach trajectory (Table 6). Indeed, the observed meteorite strewn field is parallel to the calculated asteroid ground track for masses between 1 g and 500 g (Shaddad et al. 2010). We saw in Sec. 3 that small meteorites show a south offset with respect to the ground-track, which suggests that the southward drift from winds below an altitude of 5 km is stronger than calculated from the UKMO wind model.

[Table 6 about here.]

4.4. Earth geopotential

The Earth gravity field can be expressed as an expansion in spherical harmonics (Kaula 1966). Our baseline solution only accounts for the quadrupole J_2 term. Neglecting this term and using a monopole gravity field for the Earth causes an along-track error of about 2 km and a cross-track error of 1 about km, which would move north the ground-track farther from the meteorite locations as shown by Fig. 4.

On the other hand, non-zonal and higher degree harmonics have a small effect on the impact prediction estimates. For instance, by including a full 4x4 Earth geopotential model we find a 17

m west shift along the ground-track and 3 m south shift cross-track. While these corrections are larger than numerical noise (Sec. 4.5.1), they are dwarfed by the prediction uncertainty and so they are not significant.

4.5. Smaller effects

4.5.1. Numerics

To quantify the numerical error in the propagation of the orbit of 2008 TC_3, we compared the impact trajectory to that obtained with OrbFit[9] starting from the same initial conditions and using the same force model. Since the JPL Orbit Determination Comet and Asteroid Orbit Determination Package and OrbFit use different numerical integrators, the difference between the two trajectories is a proxy for the magnitude of the numerical error. We found differences as large as 3 m, which suggests that the numerical integration error is at the few meter level.

4.5.2. Earth rotation model

The errors of the Earth Rotation Model provided by JPL's EOP files (Chin et al. 2009) are not significant. In fact, these files have a prediction accuracy requirement of 30 cm and the typical delivered accuracy is better than 17 cm, while the reconstruction error is at the centimeter level (Oliveau and Freedman 1997; Thornton and Border 2003, Chap. 3). It is worth noting that for future and longer-term impact predictions one may need to go beyond the time interval covered by EOP files. In such cases, lower fidelity Earth rotation models can be used. For instance, the 1976 IAU precession model (Lieske 1979) causes a 340 m error in the impact location estimate.

4.5.3. Nongravitational perturbations

Given the small size of 2008 TC_3, nongravitational perturbations such as solar radiation pressure (Vokrouhlický and Milani 2000) and the Yarkovsky effect (Bottke et al. 2006) could affect its trajectory. With less than two days of observation arc there is no signal of any nongravitational perturbations. To test their effect on the trajectory of 2008 TC3 we included in the force model solar radiation pressure and the Yarkovsky effect as estimated for 2009 BD, which is an object thought to have a similar size to that of 2008 TC_3 (Mommert et al. 2014). As expected, because of the short arc and short mapping times, the impact prediction is not sensitive to nongravitational accelerations. Differences in the impact location are few tens centimeters.

[9] `http://adams.dm.unipi.it/orbfit`

4.5.4. Relativity

To test the sensitivity to the relativistic model, we replaced the Einstein-Infeld-Hoffmann formulation with a lower-accuracy general relativistic model for the Sun (Damour and Deruelle 1985). Chesley et al. (2014) found that the difference between these two models is significant in modeling the trajectory of asteroid (101955) Bennu. However, for 2008 TC_3 we only obtain half-meter differences.

4.5.5. Planetary and Lunar Ephemerides

To check the sensitivity to the planetary and lunar ephemerides, we compared our baseline prediction to that obtained by used the DE405 version of JPL's Planetary and Lunar Ephemerides (Standish 1998) and found that differences are as large as 20 cm.

4.5.6. Perturbers

Finally, to test the sensitivity to main-belt perturbers we compared the baseline prediction to that obtained with no perturbations from main-belt objects. Again, differences were at the centimeter level.

5. Conclusions

By using the available 883 astrometric observations, we estimated the orbit and impact circumstances of 2008 TC_3. The asteroid reached an altitude of 100 km on 2008 Oct 7 at 02:45:30 UTC with a shallow entry angle of 21°, a relative velocity of 12.38040 km/s, and a velocity azimuth of 101°. The corresponding impact footprint is centered above the Nubian Desert in North Sudan, at an east longitude of 30.538° and a latitude of +21.087°, and its 1-σ uncertainty ellipse is 0.461 km × 0.049 km, with a semimajor axis azimuth of 104.6°.

As 2008 TC_3 approaches the sea level the projection on the ground moves east. If drag is neglected, the altitude changes at an average rate of 4.25 km/s, and east longitude and latitude change at an average rate of about $+0.11°$/s and $-0.02°$/s, respectively. The drag-free ground-track is consistent with the location of the meteorite recovered by Jenniskens et al. (2009), which are located on both sides of the ground-track.

The estimate of the 2008 TC_3 trajectory is stable with respect to different statistical treatments of the astrometric data and the length of the data arc. It is important to note that the astrometric errors become larger as the object gets closer to Earth and therefore the corresponding data-weights should be relaxed. The observation quality degradation can be explained by the increase

of the plane-of-sky motion rates, which inflate the contribution of timing errors, and of the object's brightness, which goes beyond the saturation limit and makes it difficult to accurately measure the astrometric position.

The quadrupole term (J_2) of the Earth geopotential significantly affects impact predictions. Using a monopole model for the Earth gravity shifts the ground-track north by more than 1 km and the position along the ground-track is off by more than 2 km. Non-zonal and higher order harmonics have a smaller, mostly along-track, effect within 20 m.

A simple drag model shows that the atmospheric trajectory of 2008 TC_3 is not significantly affected above 50 km of altitude. For lower altitudes drag decreases the velocity of 2008 TC_3 with respect to the impact point and causes a shift as large as a few kilometers along the ground-track at sea level. The magnitude of the atmospheric drag accelerations depends on the specific properties of the target asteroid, e.g., size, mass, and rotation state, and the impact velocity. Therefore, an object with a lower bulk density or higher impact velocity will be subject to stronger drag accelerations. Conversely, the trajectory of an asteroid larger than 2008 TC_3 with the same impact velocity will be less affected by drag and so drag can be neglected at altitudes lower than 50 km.

Acknowledgments

The authors are thankful to J. Ďurech and P. Scheirich for their help in determining the correct shape and orientation at entry of 2008 TC_3. D. Farnocchia, S. R., Chesley, and P. W. Chodas conducted this research at the Jet Propulsion Laboratory, California Institute of Technology, under a contract with NASA. The research by P. Jenniskens and D. K. Robertson is supported by the Asteroid Threat Assessment Project at NASA Ames Research Center. L. Dimare conducted this research under ESA contract No. 4000113555/15/D/MRP.

REFERENCES

Bottke, W. F., Vokrouhlický, D., Rubincam, D. P., and Nesvorný, D. (2006). The Yarkovsky and Yorp Effects: Implications for Asteroid Dynamics. *Annual Review of Earth and Planetary Sciences*, 34:157–191.

Carpino, M., Milani, A., and Chesley, S. R. (2003). Error statistics of asteroid optical astrometric observations. *Icarus*, 166:248–270.

Chesley, S. R., Farnocchia, D., Nolan, M. C., Vokrouhlický, D., Chodas, P. W., Milani, A., Spoto, F., Rozitis, B., Benner, L. A. M., Bottke, W. F., Busch, M. W., Emery, J. P., Howell, E. S., Lauretta, D. S., Margot, J.-L., and Taylor, P. A. (2014). Orbit and bulk density of the OSIRIS-REx target Asteroid (101955) Bennu. *Icarus*, 235:5–22.

Chin, T. M., Gross, R. S., Boggs, D. H., and Ratcliff, J. T. (2009). Dynamical and Observation Models in the Kalman Earth Orientation Filter. *Interplanetary Network Progress Report*, 176(27):1–25.

Damour, T. and Deruelle, N. (1985). General relativistic celestial mechanics of binary systems. I. The post-Newtonian motion. *Ann. Inst. Henri Poincaré Phys. Théor.*, 43:107–132.

Ďurech, J., Sidorin, V., and Kaasalainen, M. (2010). DAMIT: a database of asteroid models. *A&A*, 513:A46.

Farnocchia, D., Chesley, S. R., Brown, P. G., and Chodas, P. W. (2016). The trajectory and atmospheric impact of asteroid 2014 AA. *Icarus*, 274:327–333.

Farnocchia, D., Chesley, S. R., Chamberlin, A. B., and Tholen, D. J. (2015a). Star catalog position and proper motion corrections in asteroid astrometry. *Icarus*, 245:94–111.

Farnocchia, D., Chesley, S. R., Milani, A., Gronchi, G. F., and Chodas, P. W. (2015b). Orbits, Long-Term Predictions, Impact Monitoring. In Michel, P., DeMeo, F. E., and Bottke, W. F., editors, *Asteroids IV*, pages 815–834.

Folkner, W. M., Williams, J. G., Boggs, D. H., Park, R. S., and Kuchynka, P. (2014). The Planetary and Lunar Ephemerides DE430 and DE431. *Interplanetary Network Progress Report*, 196:1–81.

Jenniskens, P., Shaddad, M. H., Numan, D., Elsir, S., Kudoda, A. M., Zolensky, M. E., Le, L., Robinson, G. A., Friedrich, J. M., Rumble, D., Steele, A., Chesley, S. R., Fitzsimmons, A., Duddy, S., Hsieh, H. H., Ramsay, G., Brown, P. G., Edwards, W. N., Tagliaferri, E., Boslough, M. B., Spalding, R. E., Dantowitz, R., Kozubal, M., Pravec, P., Borovicka, J., Charvat, Z., Vaubaillon, J., Kuiper, J., Albers, J., Bishop, J. L., Mancinelli, R. L., Sandford, S. A., Milam, S. N., Nuevo, M., and Worden, S. P. (2009). The impact and recovery of asteroid 2008 TC_3. *Nature*, 458:485–488.

Kaasalainen, M. and Torppa, J. (2001). Optimization Methods for Asteroid Lightcurve Inversion. I. Shape Determination. *Icarus*, 153:24–36.

Kaula, W. M. (1966). *Theory of satellite geodesy. Applications of satellites to geodesy.* Dover Publications.

Kohout, T., Kiuru, R., Montonen, M., Scheirich, P., Britt, D., Macke, R., and Consolmagno, G. (2011). Internal structure and physical properties of the Asteroid 2008 TC_3 inferred from a study of the Almahata Sitta meteorites. *Icarus*, 212:697–700.

Kozubal, M. J., Gasdia, F. W., Dantowitz, R. F., Scheirich, P., and Harris, A. W. (2011). Photometric observations of Earth-impacting asteroid 2008 TC_3. *Meteoritics and Planetary Science*, 46:534–542.

Larson, S., Brownlee, J., Hergenrother, C., and Spahr, T. (1998). The Catalina Sky Survey for NEOs. In *Bulletin of the American Astronomical Society*, volume 30 of *BAAS*, page 1037.

Lieske, J. H. (1979). Precession matrix based on IAU /1976/ system of astronomical constants. *A&A*, 73:282–284.

Mommert, M., Hora, J. L., Farnocchia, D., Chesley, S. R., Vokrouhlický, D., Trilling, D. E., Mueller, M., Harris, A. W., Smith, H. A., and Fazio, G. G. (2014). Constraining the Physical Properties of Near-Earth Object 2009 BD. *ApJ*, 786:148.

Monet, D. G. (1998). The 526,280,881 Objects In The USNO-A2.0 Catalog. In *American Astronomical Society Meeting Abstracts*, volume 30 of *Bulletin of the American Astronomical Society*, page 1427.

Moyer, T. D. (2003). *Formulation for Observed and Computed Values of Deep Space Network Data Types for Navigation*. Wiley-Interscience.

Oliveau, S. H. and Freedman, A. P. (1997). Accuracy of Earth Orientation Parameter Estimates and Short-Term Predictions Generated by the Kalman Earth Orientation Filter. *Telecommunications and Data Acquisition Progress Report*, 129:1–10.

Roy, A. E. (2005). *Orbital motion*. Institute of Physics Publishing.

Scheirich, P., Ďurech, J., Pravec, P., Kozubal, M., Dantowitz, R., Kaasalainen, M., Betzler, A. S., Beltrame, P., Muler, G., Birtwhistle, P., and Kugel, F. (2010). The shape and rotation of asteroid 2008 TC_3. *Meteoritics and Planetary Science*, 45:1804–1811.

Seidelmann, P. K. (1982). 1980 IAU theory of nutation - The final report of the IAU Working Group on Nutation. *Celestial Mechanics*, 27:79–106.

Shaddad, M. H., Jenniskens, P., Numan, D., Kudoda, A. M., Elsir, S., Riyad, I. F., Ali, A. E., Alameen, M., Alameen, N. M., Eid, O., Osman, A. T., Abubaker, M. I., Yousif, M., Chesley, S. R., Chodas, P. W., Albers, J., Edwards, W. N., Brown, P. G., Kuiper, J., and Friedrich, J. M. (2010). The recovery of asteroid 2008 TC_3. *Meteoritics and Planetary Science*, 45:1557–1589.

Standish, E. M. (1998). JPL Planetary and Lunar Ephemerides, DE405/LE405. Technical Report IOM 312.F-98-048, Jet Propulsion Laboratory.

Swinbank, R. and O'Neill, A. (1994). A Stratosphere-Troposphere Data Assimilation System. *Monthly Weather Review*, 122:686.

Taylor, J. R. (1997). *An introduction to error analysis*. University Science Books.

Tholen, D. J. (1989). Asteroid taxonomic classifications. In Binzel, R. P., Gehrels, T., and Matthews, M. S., editors, *Asteroids II*, pages 1139–1150.

Thornton, C. L. and Border, J. S. (2003). *Radiometric Tracking Techniques for Deep-Space Navigation*. Wiley-Interscience.

Vokrouhlický, D. and Milani, A. (2000). Direct solar radiation pressure on the orbits of small near-Earth asteroids: observable effects? *A&A*, 362:746–755.

List of Figures

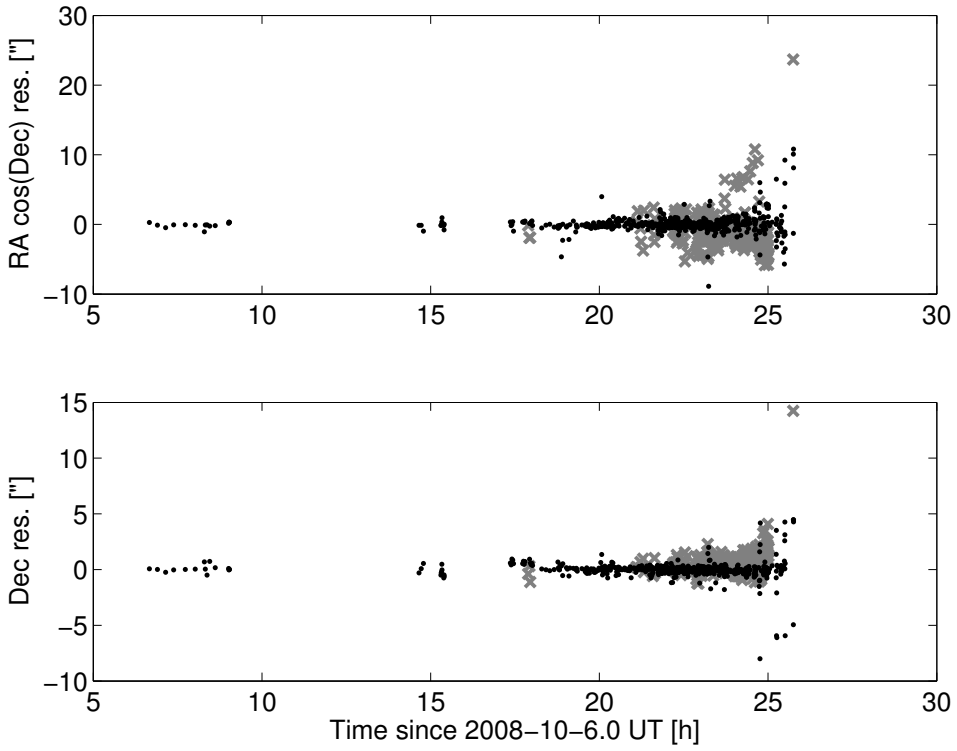

Fig. 1.— Right Ascension and Declination astrometric residuals against JPL solution 18. Black dots correspond to observations included in the fit, gray crosses to observations excluded from the fit.

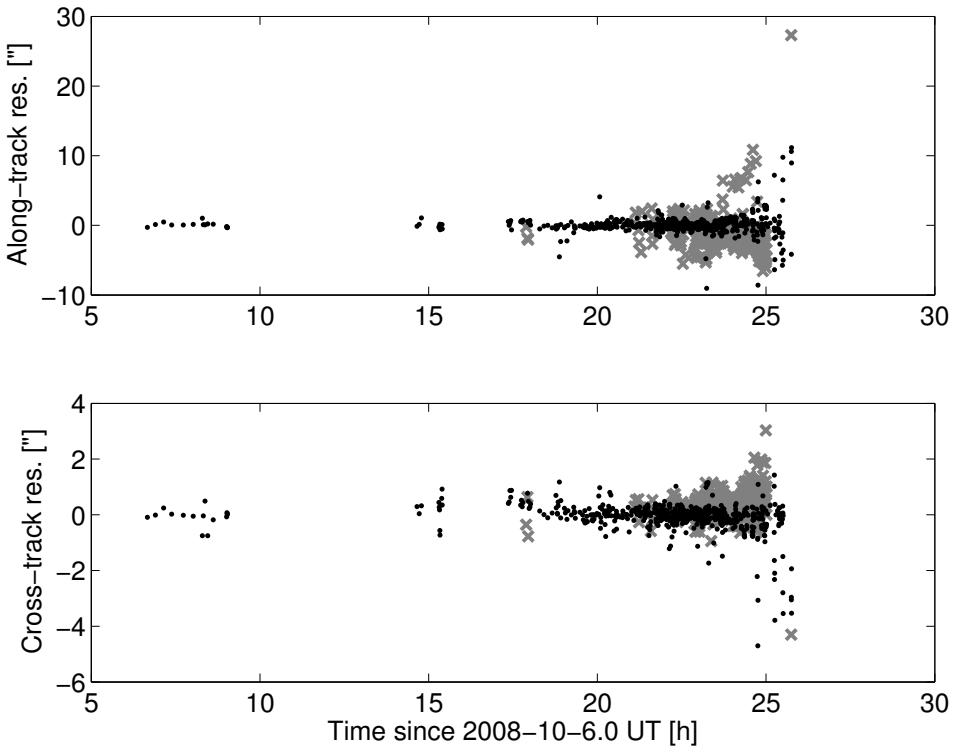

Fig. 2.— Along-track and cross-track astrometric residuals against JPL solution 18. The along-track direction corresponds to that of the plane-of-sky motion of 2008 TC_3, cross-track is the orthogonal direction. Black dots correspond to observations included in the fit, gray crosses to observations excluded from the fit.

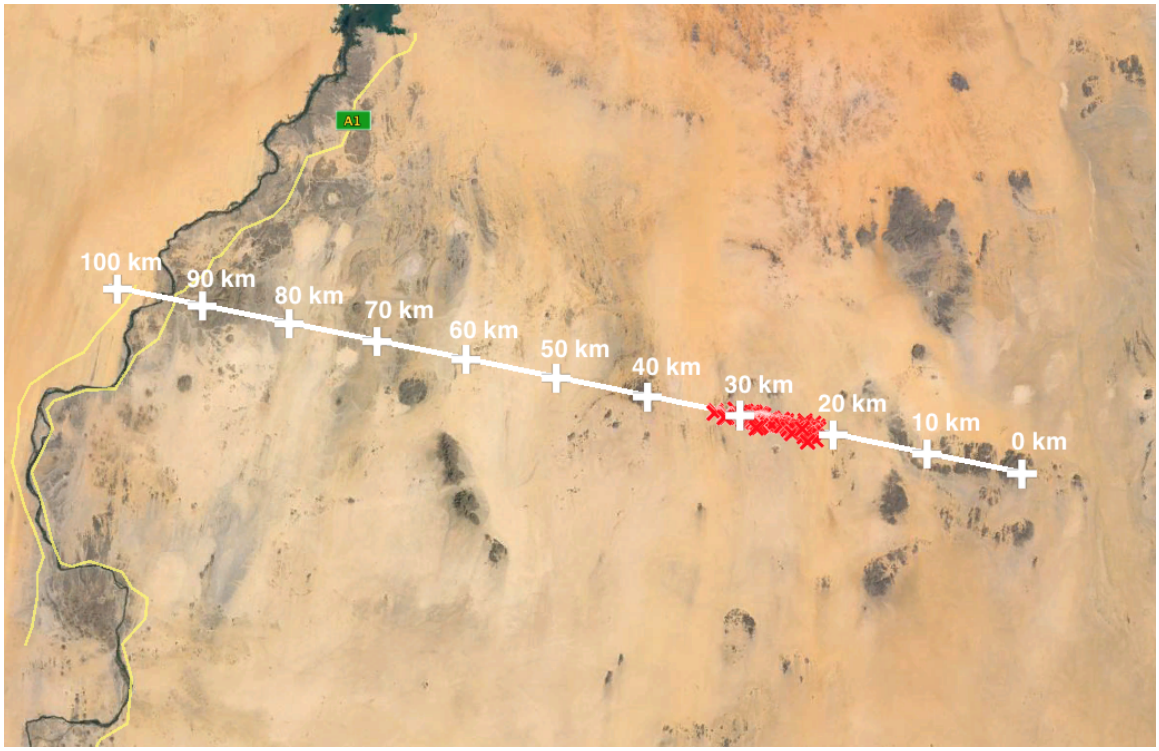

Fig. 3.— Drag-free ground-track. Red crosses correspond to the locations where meteorites were found by Jenniskens et al. (2009) and Shaddad et al. (2010).

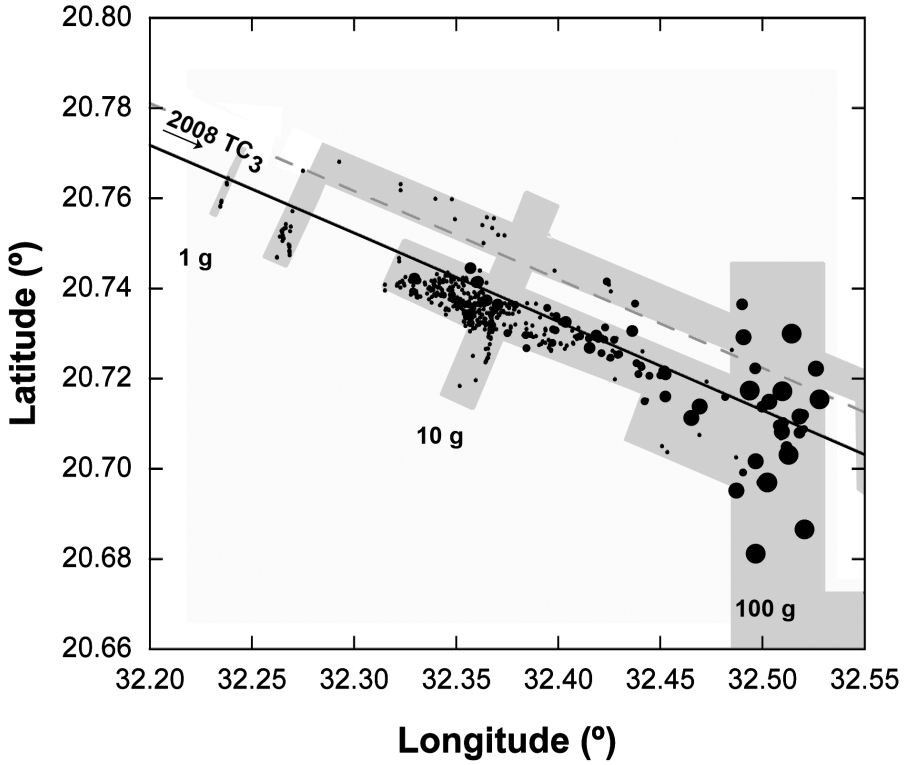

Fig. 4.— Close-up of the meteorite locations (black dots) relative to the ground-track (solid line). The areas searched by Jenniskens et al. (2009) and Shaddad et al. (2010) are in gray, the dashed line is the ground-track used by Jenniskens et al. (2009), which did not include Earth's J_2. Larger dots correspond to larger meteorite sizes.

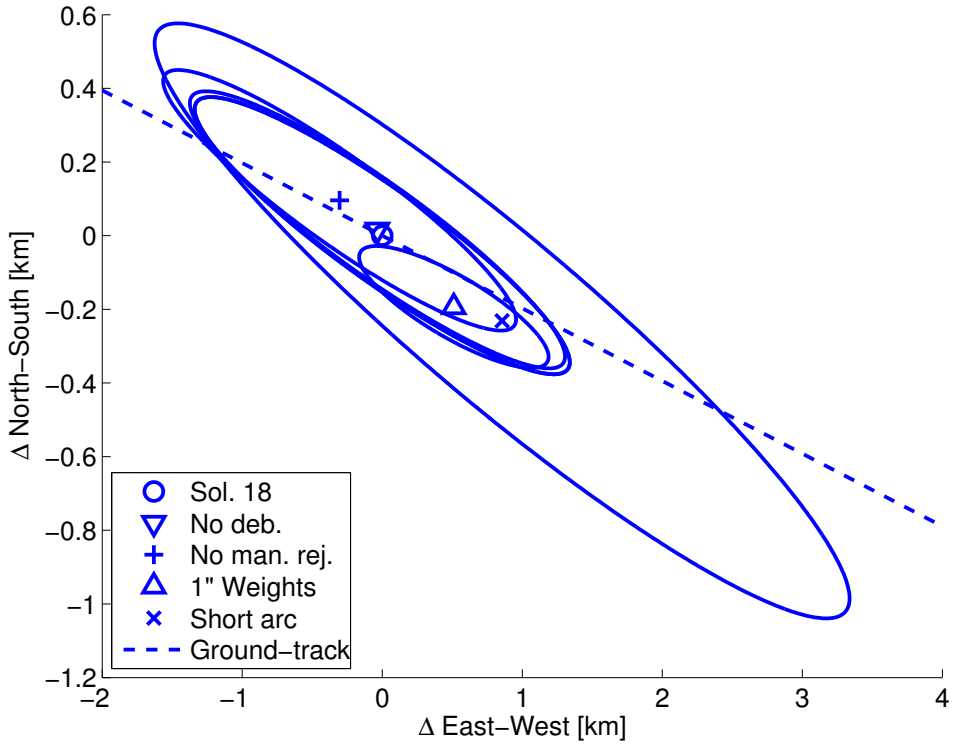

Fig. 5.— Impact location 3-σ error ellipses for different orbital solutions: JPL solution 18, no star catalog debiasing, no manual rejection of outliers, uniform weighting at $1''$, shorter arc with data until 2008-Oct-7.0 UTC. The impact locations correspond to an altitude of 100 km and the origin corresponds to JPL solution 18, i.e., an East Longitude of 30.5380° and a Latitude of 21.0871°. Note that the axes do not use the same scale.

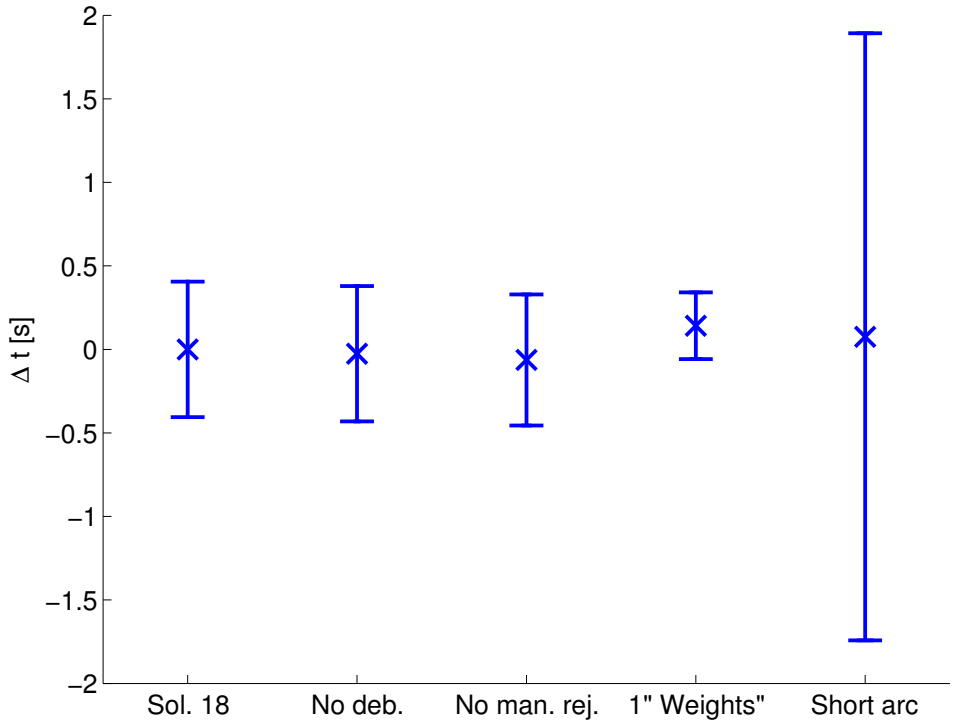

Fig. 6.— Time of impact and 3-σ error bars for different orbit solutions: JPL solution 18, no star catalog debiasing, no manual rejection of outliers, uniform weighting at $1''$, shorter arc with data until 2008-Oct-7.0 UTC. The impact time corresponds to an altitude of 100 km and the origin of the y-axis is 2008-Oct-07 02:45:30.32 UTC.

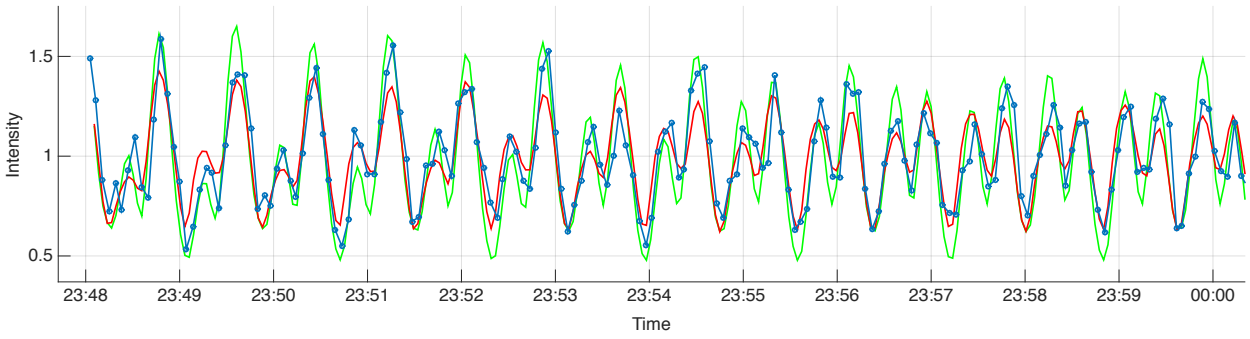

Fig. 7.— Observed and calculated lightcurve of 2008 TC_3 for adopted shape model. Blue dots show the observations from Clay Center Observatory (Kozubal et al. 2011), the red line is the projected cross-sectional area for the shape model viewed from Earth, while the green line represents the reflected sun light.

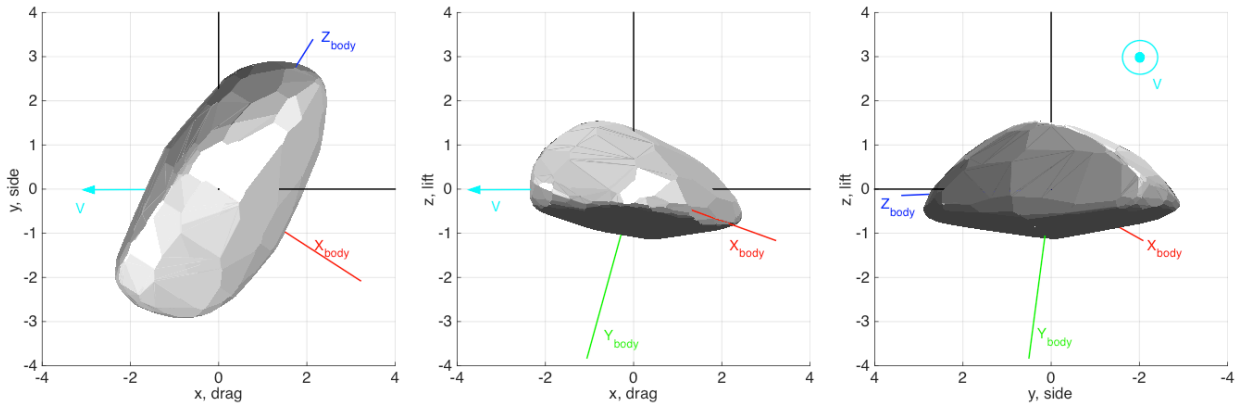

Fig. 8.— Orientation of the shape model in the Wind Frame, defined as Drag, Side, and Lift directions.

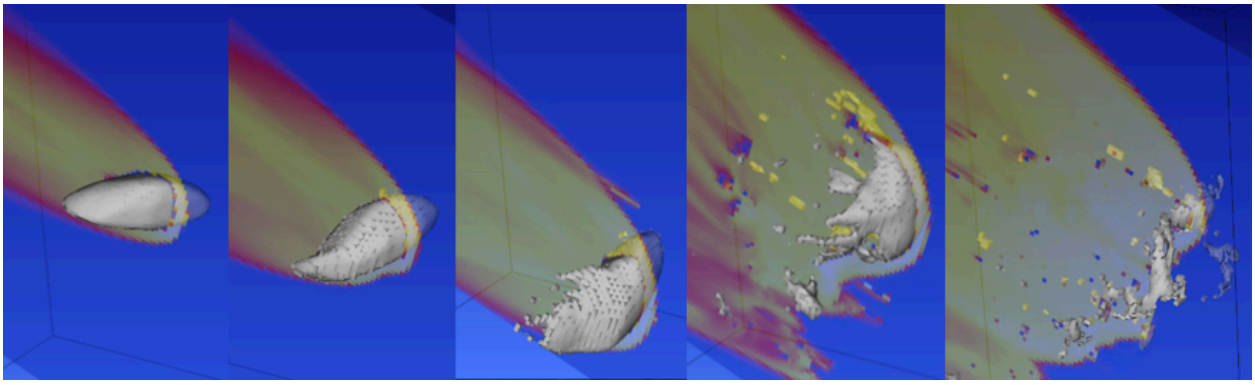

Fig. 9.— Homogeneous strengthless model of atmospheric entry of asteroid 2008 TC3. This model was used to calculate lift, drag, and side force coefficients prior to significant disruption.

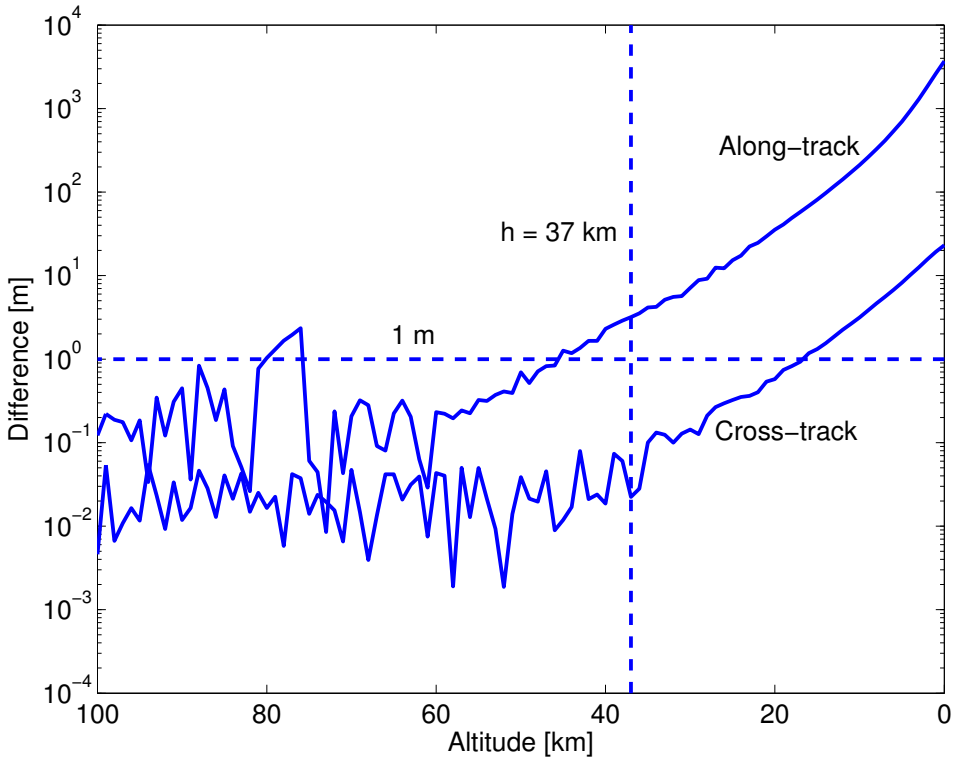

Fig. 10.— Along-track and cross-track shifts caused by atmospheric drag. The vertical dashed line represents the altitude at which 2008 TC_3 exploded, the horizontal dashed line corresponds to 1 m as guide for the numerical integration error.

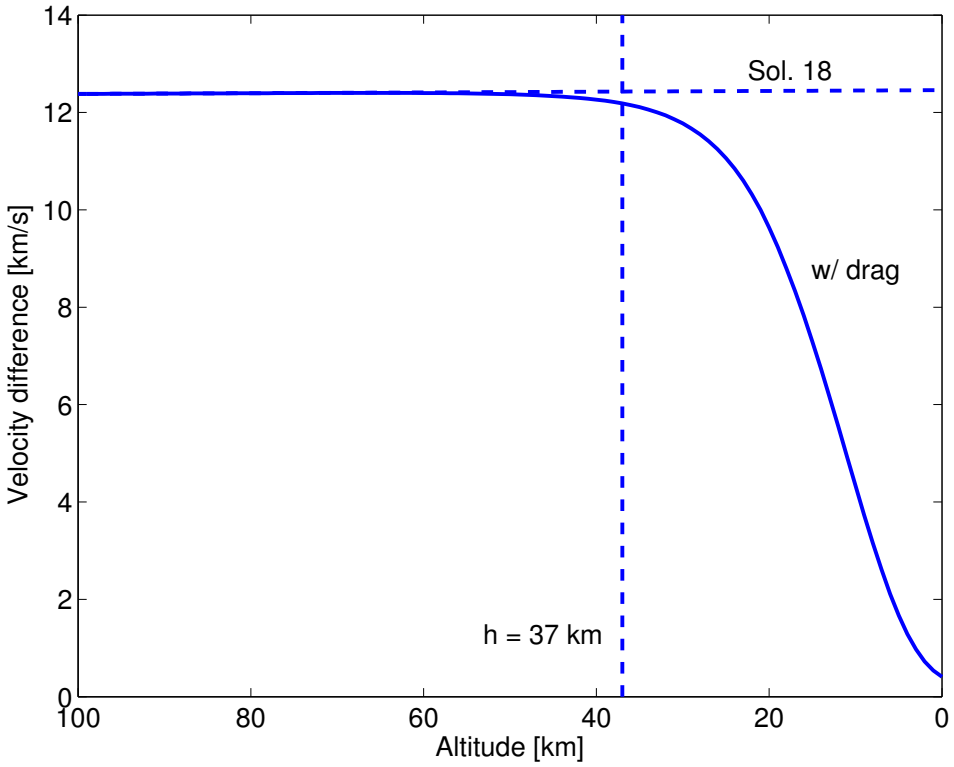

Fig. 11.— Variations of the magnitude of the velocity relative to impact point caused by atmospheric drag. The vertical dashed line represents the altitude at which 2008 TC_3 exploded.

List of Tables

Table 1: JPL solution 18. The orbital elements are ecliptic heliocentric and error bars correspond to 1-σ formal uncertainties.

Epoch TDB	2008 Oct 07.0
Eccentricity	0.3120674 ± 0.0000048
Perihelion distance	0.8999569 ± 0.0000012 au
Time of perihelion TDB	2008 Nov 20.39885 ± 0.00013 d
Longitude of node	194.1011436° ± 0.0000015°
Argument of perihelion	234.448925° ± 0.000056°
Inclination	2.542215° ± 0.000035°

Table 2: Impact parameters of 2008 TC_3 at an altitude of 100 km for JPL solution 18. The reported velocity is relative to the body-fixed position of the impact location. Azimuth and elevation correspond to the direction from which 2008 TC_3 is seen from an observer at the impact location. Error bars correspond to 1-σ formal uncertainties.

Impact parameters	
Time UTC	2008 Oct 07 02:45:30.33 ± 0.14 s
Latitude	$21.0871^\circ \pm 0.0011^\circ$
East Longitude	$30.5380^\circ \pm 0.0043^\circ$
Velocity	12.380399 ± 0.000057 km/s
Azimuth	$281.0968^\circ \pm 0.0017^\circ$
Elevation	$20.8332^\circ \pm 0.0034^\circ$
Impact ellipse	
1-σ semimajor axis	0.461 km
1-σ semiminor axis	0.049 km
Major axis azimuth	104.6°
1-σ north-south uncertainty	0.125
1-σ east-west uncertainty	0.446

Table 3: Drag-free ground-track. The reported velocity is relative to the body-fixed location of the impact location. Azimuth and elevation correspond to the direction from which 2008 TC_3 is seen from an observer at the impact location.

Alt km	Time UTC	Lat °	E Long °	Velocity km/s	Az °	El °
100	02:45:30.32	21.0871	30.5380	12.380	281.10	20.83
90	02:45:32.60	21.0417	30.7834	12.388	281.19	20.68
80	02:45:34.90	20.9955	31.0312	12.396	281.29	20.52
70	02:45:37.21	20.9484	31.2813	12.403	281.38	20.36
60	02:45:39.53	20.9005	31.5338	12.411	281.48	20.19
50	02:45:41.87	20.8516	31.7887	12.419	281.57	20.03
40	02:45:44.23	20.8018	32.0462	12.427	281.67	19.87
30	02:45:46.61	20.7511	32.3062	12.435	281.77	19.70
20	02:45:49.00	20.6994	32.5688	12.442	281.87	19.53
10	02:45:51.42	20.6467	32.8342	12.450	281.97	19.36
0	02:45:53.85	20.5930	33.1023	12.458	282.07	19.19

Table 4: Orientation of 2008 TC_3 in the equatorial direction (J2000) frame given in right ascension and declination and the equivalent direction cosine matrix (DCM), and also the DCM in the Ground Range Frame (GRF).

J2000 Equatorial Direction		
Body-Axis	RA	Dec
X	340.76°	+39.29°
Y	275.42°	−27.02°
Z	29.63°	−38.80°
J2000 Direction Cosine Matrix		
X	Y	Z
0.73076	0.084118	0.67744
−0.25508	−0.88684	0.38528
0.63319	−0.45435	−0.62661
Ground Range Frame DCM		
X	Y	Z
0.85472	0.091703	0.51093
−0.51893	0.12594	0.84549
0.013189	−0.98779	0.15523

Table 5: Drag coefficient, side force and lift at different times ($t = 0$ corresponds to $h = 60$ km).

Time [s]	C_D	C_Y	C_L
0.1	1.73	0.897	−0.0534
0.2	1.97	0.067	0.0801
0.5	1.89	−1.01	0.0267
1.0	2.40	−1.00	0.0553

Table 6: Displacement of spherical meteorites of density ρ of 2.2 g/cm^3 and 3.4 g/cm^3, falling from 33 km altitude to an adopted ground altitude of 490 m, with initial speed and direction of 2008 TC_3.

Mass	Time	Impact velocity	Δ(N-S) [km]	
kg	s	m/s	$\rho = 2.2$ g/cm^3	$\rho = 3.4$ g/cm^3
100	45	241	+0.09	+0.03
10	69	163	+0.15	+0.16
1	103	107	+0.10	+0.11
0.1	156	71	+0.07	+0.06
0.01	235	48	+0.11	+0.10
0.001	352	33	+0.09	+0.10